Drug Design, Development and Therapy

Dovepress
Taylor & Francis Group

Open Access Full Text Article

ORIGINAL RESEARCH

Wedelolactone Ameliorates Ischemic Stroke by Inhibiting Oxidative Damage and Ferroptosis via HIF-1α/SLC7A11/GPX4 Signaling

Xingru Tao*, Meina Zhao*, Kai Gao*, Wei Zhang, Dong Xu, Wangting Li, Fei Mu, Rui Lin, Chao Guo, Ruili Li, Jingwen Wang

Department of Pharmacy, Xijing Hospital, Fourth Military Medical University, Xi'an, 710032, People's Republic of China

*These authors contributed equally to this work

Correspondence: Jingwen Wang, Email wangjingwen8021@163.com

Purpose: Wedelolactone (Wel), a furocoumarin compound extracted from the medicinal plant *Eclipta prostrata L*. has been shown to exhibit significant neuroprotective effects. However, the potential of Wel to improve ischemic stroke (IS) and the underlying mechanisms remain unclear.

Methods: The middle cerebral artery occlusion and reperfusion (MCAO/R) and oxygen-glucose deprivation/reoxygenation (OGD/R) were established to evaluate the potential neuroprotective of Wel. Neurological function, brain infarct volume, brain swelling, and histopathological staining were analyzed to demonstrate the therapeutic efficacy of Wel. The occurrence of ferroptosis was confirmed by quantifying the levels of ROS and Fe^{2+}, and by examining the ultrastructural features of cells. The binding affinity between Wel and HIF-1α was evaluated using Molecular docking. Immunofluorescence and Western blot analyses were conducted to explore the regulation of Wel on the HIF-1α/SLC7A11/GPX4 pathway. Finally, the expression of HIF-1α was down-regulated to verify whether Wel exerts neuroprotection by modulating HIF-1α to inhibit ferroptosis of cells.

Results: The results demonstrated that Wel effectively inhibit neuron ferroptosis after MCAO/R in a dose-time-dependent manner, thereby alleviating brain injury. Moreover, at the cellular level, Wel significantly reduced the accumulation of Fe^{2+} and ROS after OGD/R. Further investigation revealed that Wel might inhibit neuronal ferroptosis and improve IS by promoting the nuclear translocation and accumulation of HIF-1α, subsequently regulating the expression of downstream proteins SLC7A11 and GPX4. Notably, the inhibitory effect of Wel on ferroptosis was markedly attenuated by HIF- 1α siRNA in OGD/R PC12 cells.

Conclusion: Our discovery revealed that the Wel could alleviate IS by inhibiting oxidative damage and ferroptosis via HIF-1α/SLC7A11/GPX4 signaling pathway. Wel may represent a promising active compound for anti-IS, while also providing novel insights into the elucidation of its molecular mechanisms and potential clinical implications.

Keywords: Wedelolactone, ischemic stroke, ferroptosis, HIF-1α/SLC7A11/GPX4 pathway

Introduction

Ischemic stroke (IS) is the most common type of stroke and is one of the diseases with the highest disability and mortality rates worldwide.[1] Currently, commonly used treatments for IS include pharmacological thrombolysis or interventional techniques, which can rapidly restore perfusion to the blood vessels.[2] However, its application is severely limited by the narrow treatment time window and the risk of bleeding.[3] Consequently, it is of particular significance to seek and develop effective alternative drugs with few side effects for the treatment of cerebral ischemia/reperfusion injury (CI/RI).

The types of cell death encompass pyroptosis, necroptosis, apoptosis, and ferroptosis.[4] The characteristics of ferroptosis are iron dependence and excessive lipid peroxidation accumulation.[5] Disruption of antioxidant system X_C^-/GSH/GPX4 is a significant mechanism leading to ferroptosis. System X_C^- is an amino acid antiporter that exchanges and it is composed of transporter subunit SLC7A11 and regulatory subunit SLC3A2. Cystine is rapidly reduced to cysteine after entering the cell

Received: 15 April 2025
Accepted: 25 July 2025
Published: 8 August 2025

Graphical Abstract

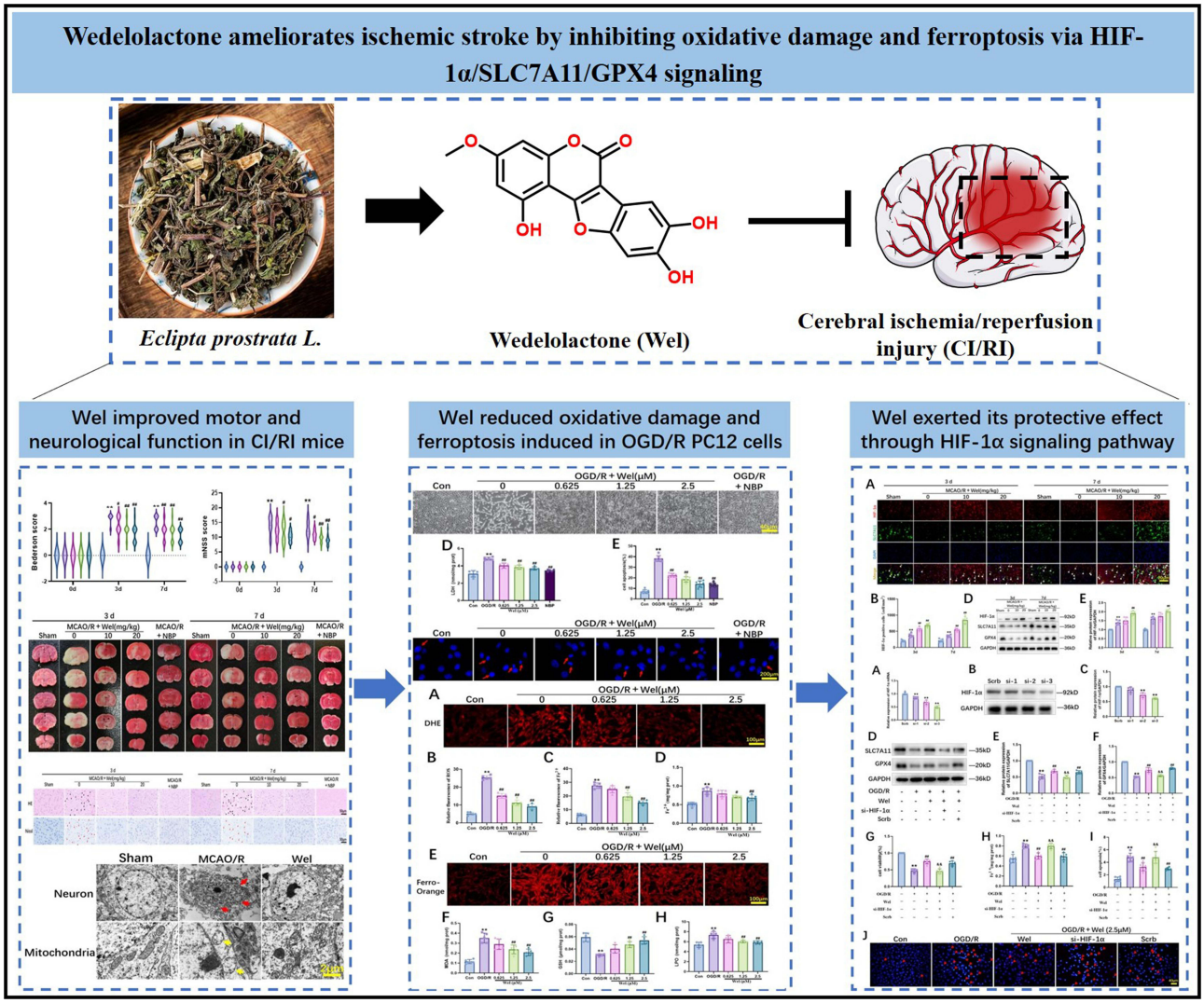

and is used for the synthesis of endogenous GSH.[6] Glutathione (GSH) is a crucial intracellular antioxidant and also the substrate for the synthesis of glutathione peroxidase 4 (GPX4). GPX4 is a key regulatory factor of ferroptosis, which prevented cellular lipid peroxidation by converting lipid peroxidation into non-toxic alcohols.[7] It has been reported that iron accumulation exacerbates neuronal injury during reperfusion.[8] Hence, comprehending the role of ferroptosis in CI/RI might be a novel breakthrough in the IS therapy.

Hypoxia-inducible factor-1α (HIF-1α) is ubiquitously expressed in mammalian cells. Under normal conditions, HIF-1α undergoes hydroxylation catalyzed by prolyl hydroxylase (PHD), followed by ubiquitination via an E3 ubiquitin ligase complex, and is ultimately degraded by the 26S proteasome. In contrast, under hypoxic conditions, the inactivation of PHD results in the stabilization and accumulation of HIF-1α within cells, enabling it to regulate the cellular response to hypoxia.[9] Previous studies have demonstrated that following ischemic-hypoxic brain injury, HIF-1α is promptly activated and exerts neuroprotection through multiple pathways, including the regulation of glucose metabolism, angiogenesis, and apoptosis.[10] Recent studies have shown that HIF-1α has the potential to regulate SLC7A11 and thereby inhibit ferroptosis in liver fibrosis and kidney diseases.[11–13] Meanwhile, the protein expression of SLC7A11 in the brain tissue of HIF-1α knockout rats was simultaneously decreased.[14] Therefore, we hypothesize that in the pathological context of ischemic stroke, HIF-1α

may be involved in the SLC7A11/GPX4-mediated ferroptosis process. However, whether this hypothesis holds true remains to be determined.

Wedelolactone (Wel) is a kind of small molecule furanocoumarins compound extracted from the medicinal plants *Eclipta prostrata L*. It possesses the functions of liver protection, anti-inflammation, blood sugar reduction, and neuroprotection, and is frequently utilized in the treatment of coronary heart disease, liver disease, nervous system diseases, etc.[15] Previous studies have reported that Wel could alleviate lung injury and liver injury by regulating the ferroptosis pathway.[16,17] However, it remains unclear whether Wel can regulate the occurrence of ferroptosis in neurological diseases. Chen et al conducted a pharmacokinetic study of Wel using UPLC-Q-TOF/MS, and found that its time to peak concentration (T_{max}) was 0.5 hours, and it was significantly distributed in tissues.[18] Wei et al administered the extracts of *Eclipta prostrata L*. to Alzheimer's disease model rats. The results demonstrated that Wel was detected in both the brain tissue and serum of the rats, suggesting that Wel could exert neuroprotective effects by crossing the blood-brain barrier.[19] Muke et al also found that extracts of *Eclipta prostrata L*. reduced the level of neuroinflammation in the hippocampal region of the brain.[20] Although Yang's research initially revealed that Wel could ameliorate OGD/ R-induced ferroptosis at the cellular level by regulating GPX4, the lack of in-depth mechanism research and in vivo evidence makes this conclusion insufficiently objective and comprehensive.[21] Therefore, further research is warranted to comprehensively assess the protective efficacy of Wel against CI/RI.

This study comprehensively demonstrated the effect of Wel in improving CI/RI through MCAO/R in vivo and OGD/R in vitro models. And it was proved for the first time that the neuroprotective effect of Wel is closely related to ferroptosis mediated by the HIF-1α/SLC7A11/GPX4 pathway. This research was expected to provide a scientific basis for the development of Wel and also offer preclinical evidence for the therapeutic potential of Wel.

Materials and Methods

Chemicals and Reagents

Wedelolactone (purity≥98%) was gained from Baoji chenguang Co., Ltd (Shaanxi, China). Butylphthalide (NBP) was gained from CSPC Pharmaceuticals Co., Ltd (Hebei, China). Corn oil (HY-Y1888) was purchased from MedChemExpress. Antibodies against HIF-1α (BD-PT2133) and SLC7A11 (BD-PT8130) were gained from Biodragon (SuZhou, China). Antibodies against GPX4 (67,763-1-Ig) and GAPDH (60004-1-Ig) were gained from Proteintech (WuHan, China). The MDA (ml092884), LDH (ml092588), LPO (ml092623), GSH (ml076450), and GPX4 (ml057982) kits were gained from Enzyme-linked Biotechnology Co., Ltd (ShangHai, China). Hoechst 33258 (C0003) and ROS (S0063) kit and was gained from Beyotime Biotechnology Co., Ltd (ShangHai, China). The Fe^{2+}(BC5415) kit was gained from Solarbio Science & technology Co., Ltd (BeiJing, China). The HIF-1α siRNA was designed and synthesized in Haixing Biosciences company.

Animals

Adult male C57BL/6 mice age 6–8 weeks and weighing 20–25g were acquired from the Experimental Animal Center of the Fourth Military Medical University (Xi'an, China). All animal experiments were performed in accordance with the National Institutes of Health Guide for the Care and Use of Laboratory Animals and were approved by the Institutional Animal Ethics Committee of Fourth Military Medical University (Ethical approval number: KY20230626). Mice were placed in a specific pathogen-free environment, with the temperature maintained at 26 ± 2°C and the humidity maintained at 55 ± 10%.

Establishment of MCAO/R Model

Employing the formerly reported approach, namely by inducing CI/RI injury with the middle cerebral artery occlusion/ reperfusion (MCAO/R) model.[22] Briefly, the mice were continuously anesthetized with 2% isoflurane, an incision was made along the anterior median line of the neck, and the common carotid artery (CCA) was progressively dissected and fully exposed, with the vagus nerve, internal carotid artery (ICA), and external carotid artery (ECA) being carefully separated. The CCA and ECA were ligated, and the suture was inserted through the CCA into the middle cerebral artery (MCA) (approximately 10 to 11 mm), resulting in cerebral ischemic on one side of the brain. In the sham-operated group of mice, only the skin and subcutaneous tissues were incised, without any other damage. The mice were placed on a 37°C

warming pad. When the mice awoke, they were returned to their cages. After 2 hours of embolization, the suture was removed for reperfusion.

Experimental Design and Drug Administration

All male mice were randomly divided into groups by means of the random number table method, and all operators were blinded. They were randomly divided into the Sham group (n=31, without treatment): Only the skin incision and carotid artery dissection were performed, without the insertion of suture. The MCAO/R group (n=31, without treatment): The MCAO/R model was implemented using the suture insertion method. Wel group (n=31, 10 mg/kg, with treatment): In addition to MCAO/R surgery, the Wel (10 mg/kg) were administered by once daily for 3 or 7 days. Wel group (n=31, 20mg/kg, with treatment): In addition to MCAO/R surgery, the Wel (20 mg/kg) were administered by once daily for 3 or 7 days. NBP group (n=23, 25mg/kg, positive drug, with treatment): In addition to MCAO/R surgery, the NBP (25mg/kg) were administered by once daily for 3 or 7 days. The dosages of Wel and NBP were determined based on prior publications from our research group and the results of preliminary experiments.[22,23] The drug was dissolved in corn oil prior to administration. The drug was administered by i. p. injection after MCAO/R. The mice in the Sham and MCAO/R group were administered corn oil once a day according to their body weight.

Neurological Deficits, Brain Infarct Volume and Brain Water Content Assessment

Employing the Bederson score, modified Neurological Severity Score (mNSS), corner test and sticky label test to comprehensively assess the neural function of mice following CI/RI at 0d, 3d and 7d. The Bederson score was categorized into a 4-point scale, where 0 denotes no apparent symptoms, 1 indicates forelimb flexion, 2 represents diminished lateral push resistance with forelimb flexion, 3 signifies reduced lateral push resistance with forelimb flexion and spontaneous rotation, and 4 corresponds to loss of consciousness. Higher scores reflect more severe injuries. The mNSS was quantified using an 18-point scale, which encompassed assessments of motor function, sensory perception, balance, and reflexes. Specific protocols were adapted from previous studies.[24] Scores ranging from 1 to 6 indicate mild impairment, 7 to 12 denote moderate impairment, and 13 to 18 represent severe impairment. For the corner test, the mouse was positioned in a corner at a 30° angle. As the mouse moved into the depth of the angle, both sides of its whiskers made contact with the cardboard, prompting it to turn either left or right. Normal mice exhibited no directional preference, whereas CI/RI mice demonstrated a tendency to turn toward the undamaged side (the right side). The trial was conducted 20 times, and the number of rightward turns was recorded. The percentage of rightward turns in mice was calculated using the formula: (number of rightward turns / total number of turns) × 100%. A higher percentage indicated a more severe injury.[25] For the sticky label test, a circular adhesive label with a diameter of 5 mm was affixed to the mouse's front paw, and the time required for the mouse to remove the label was documented. Longer durations correspond to greater motor function deficits.[26]

When the neurological function score of the mouse was completed, the brain tissue was collected at 3d and 7d immediately. After rinsing with precooled saline, immediately put it into -20°C refrigerator. After 30 min, the brain slices were removed and cut into 2mm. The brain slices were placed in 2% TTC staining solution, incubated at 37°C in the dark for 30 min, and then fixed with 4% paraformaldehyde. Photographs were taken and the results were analysed.[27] At the same time, the brain tissues of each group were taken, immediately rinsed with physiological saline, and after drying, the wet weight (WW) was weighed. Subsequently, they were placed in a constant temperature oven at 70 °C, and after 48 hours, the dry weight (DW) was taken out and weighed. The brain water content (BWC)= (WW - DW)/WW × 100%.[28]

Hematoxylin and Eosin (H&E) and Nissl Staining

The brain tissue samples were taken for routine dehydration, wax immersion, paraffin embedding, and conduct tissue paraffin block sectioning with a thickness of 3 to 5 μm. After dewaxing and dehydrating, hematoxylin and eosin staining were performed, the slices were sealed. Ultimately, the morphological alterations of the neurons were observed under the microscope and photographed. At the same time, brain sections are employed for Nissl staining. The Nissl-stained positive cells on the ischemic side were observed under microscope. Image J software was utilized for result analysis.

Transmission Electron Microscopy

The injured part of fresh brain tissue was cut into $1\times1\times1cm^3$ cubes, which was immediately fixed in glutaraldehyde, rinsed with phosphoric acid, fixed with Osmic acid, gradient dehydration with ethanol, and embedded. Then it was polymerized in the constant temperature oven, semi-thin positioning and ultra-thin slicing machine, and uranium acetate-lead citrate double staining. Finally, the morphological changes of neurons and mitochondria in brain tissue were observed under transmission electron microscope.

Immunofluorescence

The brain tissue was immersed in 4% paraformaldehyde for 2 hours, dehydrated in a gradient of ethanol, cleared in xylene, embed in paraffin, and section. Dewax in xylene, rehydrate in different concentrations of ethanol, and wash in PBS. Block with 10% normal goat serum at room temperature for 1 hour, incubate the sections with primary antibody rabbit anti-GPX4 (1:500), anti-HIF-1α (1:200) or anti-SLC7A11 (1:200) overnight at 4°C. Wash with PBS 3 times, counterstain the nuclei with DAPI-containing anti-fluorescence quenching agent, and mount the slides. Observe and photograph under a fluorescence microscope. Analyze the fluorescence pictures using Image J software.

Detection of GSH, LDH, MDA, LPO, Fe^{2+} and GPX4 in Brain Tissue and Serum

After anesthetizing the mice, blood was collected from the eye socket, left at room temperature for 30 minutes, centrifuged at 2500g for 20 minutes, the supernatant was collected and stored at 4°C. The cerebral hemisphere corresponding to the side of the fresh infarct was resected, rinsed with pre-cooled PBS, cut into pieces, placed in a centrifuge tube, added with RIPA lysis buffer and clean steel beads, shaken in a tissue crusher to fully grind. After removal, centrifuged at 4°C 12000g for 15 minutes, and collected the supernatant. The levels of GSH, LDH (Lactate Dehydrogenase), MDA (Malondialdehyde), LPO (Lipid peroxidation), Fe^{2+} (Ferrous iron) and GPX4 were detected simultaneously in serum and brain tissue homogenates. Test strictly in accordance with the instructions of the corresponding assay kit.

Cell Culture and Drug Concentration Screen

PC12 cells were donated by department of pharmacy of Xijing Hospital. The use of the PC12 cells have been approved by the Research Ethics Committee of Xijing Hospital. The cells were cultured in DMEM high glucose medium, and were placed in a constant temperature incubator at 37 °C and 5% CO_2, and the medium was replaced every 2 days.

The cell survival rate was detected by CCK-8 kit to screen the optimal concentration of drug administration. The cells were seeded in a 96-well plate with a density of 5×10^4/well, and the Wel administration gradient was set to 0.625, 1.25, 2.5, 5, 10, 20, 40, 80 μM, while the control group was set. After the cells were attached, with the intervention of Wel for 24 hours, and thereafter the cell viability was determined.

Oxygen-Glucose Deprivation/Reoxygenation (OGD/R) and Cell Viability Assay

The preparation method of OGD/R model refers to the previous screening method of our group. In brief, complete DMEM medium was discarded, and replaced it with sugar-free DMEM, and then PC12 cells were cultured in a hypoxia incubator chamber (5% CO2, 95% N2,37°C) for 5 hours. After OGD, substituted the sugar-free DMEM medium with the complete medium and continued to culture for 24 hours in the normal incubator.

The experiment is divided into the control group, OGD/R group, Wel (0.625, 1.25 and 2.5 μM) and NBP (10 μM) groups.[29] The cells of the control group were cultured at 37 °C in CO_2 incubator, and the remaining groups were treated according to the aforementioned OGD/R method. After OGD, the sugar-free medium was changed to different concentrations of Wel or NBP medium, and the cells were incubated for 24 hours.

Hoechst 33258 Staining

After modeling and administration, the cells were washed gently with PBS. The morphology of the cells was observed under light microscope and photographed. After that, the cells were fixed with 4% paraformaldehyde for 1 h, then stained with Hoechst 33258 staining solution for 1 h, and the cell morphology was observed under fluorescence microscope.

Lipid ROS Production and Intracellular Iron Measurements

The cells were inoculated on the six-hole plate at the density of 1×10^5/mL. After the cells adhered to the wall, the above modeling and drug treatment were performed. The cells were washed twice with PBS, added with 10μM dihydroethidium staining solution prepared at 1:1000, and incubated at 37 °C in a constant temperature incubator with 5% CO_2 for 20 minutes in the dark. The dihydroethidium staining solution was discarded and washed three times with PBS. Then they were observed, photographed and recorded under a fluorescence confocal microscope. In the same way, 1 μM Ferr-orange staining solution was added to each well, diluted with serum-free medium, cultured in a constant temperature incubator at 37 °C and 5% CO_2 for 1h, and then ROS staining was performed, and photographed and recorded under a fluorescence confocal microscope.

Detection of GSH, LDH, MDA, LPO and Fe^{2+} in PC12 Cells

The cells were cultured in T75 cm^2 culture flasks. After completing the above cell modeling and drug treatment, cells were lysed and the lysate was collected. The levels of GSH, LDH, MDA, LPO, and Fe^{2+} were detected in strict accordance with the operation steps described in the manual.

HIF-1α Targeted RNA Transfection

At 50% confluence, PC12 cells were transfected with small interfering RNAs (siRNAs) targeting HIF-1α. The siRNA sequences were as follows: HIF-1α: F: 5'-GAGCUCCCAUCUUGAUAAATT-3', R: 5'-UUUAUCAAGAUGGGAGCUCTT-3'. Before transfection, cells were intervened with Opti-MEM™ for 2h. Then, the HIF-1α siRNA (50nM per well) and the lipofectamine 2000 were added into the culture medium for transfection for 8h. At the end of the intervention, OGD/R experiments were performed. After 48h, the transfection efficiency was evaluated by detecting HIF-1α mRNA and protein expression.

Quantitative Reverse Transcription PCR

The total RNA of PC12 cells were extracted, then 2ug RNA was reverse transcribed into cDNA using commercial kits. The final concentration of primers was 0.4μM, GAPDH was used as the internal parameter, and PCR efficiency was optimized and the products were produced. To ensure reaction specificity, the relative expression was calculated using 2-ΔΔCt method. The sequences of primers were as follows: GAPDH: F: 5'-TACTCGCGGCTTTACGGGT-3'; R: 5'-CTGGCACTGCA CAAGAAGATG-3'.

Western Blotting

The cerebral hemisphere on the infarcted side and PC12 cells were obtained. RIPA lysates containing PMSF and phosphatase inhibitors were added, respectively. They were incubated on ice for 30 minutes, centrifuged at 4°C for 15 minutes, and the supernatants were collected. The BCA protein concentration kit was used to determine the concentration of the sample. After quantification and denaturation, it was used for Western blotting. The protein samples were separated in SDS-PAGE gel at a dose of 20 μg per well. Next, the protein was transferred to the PVDF membrane, sealed with 5% skim milk at room temperature for 2 hours. Then, they were incubated with GAPDH, HIF-1α, SLC7A11, GPX4 first antibody, respectively, and kept refrigerated overnight in a 4°C refrigerator. Finally, they were incubated with the corresponding secondary antibody at room temperature for 2h. The bands were visualized using the Chemidoc™ imaging system (BIO RAD), and the gray-scale intensity of the bands was quantitatively analyzed using Bio-Bad software.

Molecular Docking Study

The 2D chemical structure formula of Wel was obtained from PubChem database and transformed into MOL2 format by ChemBioDraw software.[30] At the same time, the 3D structure of the target protein HIF-1α was downloaded from PDB database, and the target ligands and non-protein molecules were removed by PyMol software.[31] Use AutoDock software to convert the format of Wel and HIF-1α to PDBQT, and run AutodockVina program for docking. Finally, the interaction between Wel and HIF-1α was visualized using Discovery Studio software.

Statistical Analysis

The data analysis was conducted using GraphPad Prism 9.0 software, and the parameter values were expressed as mean ± standard deviation ($\bar{x}$±s). Each experiment was conducted independently. To minimize potential bias, all behavioral assessments, histologic analyses, and data quantification were carried out by investigators blinded to the trial-group assignments. Group labels were anonymized during both data collection and analysis to ensure objectivity. The preset statistical power is 80%, and the significance level $\alpha = 0.05$ (two-sided). The assumption of normal distribution and homogeneity of variance was verified for all datasets. For the purpose of comparing the differences among two or more groups, one-way ANOVA and Tukey's test are employed for analysis. $P < 0.05$ indicated statistically significant differences.

Results

Wel Differentially Improved Neurological Dysfunction in the MCAO/R Mice

Wedelolactone is a furan coumarin compound (Figure 1A). Figure 1B is the flow chart of this experiment. All mice underwent training to develop the ability to stabilize themselves on the balance beam and remove adhesive stickers before the start of the experiment. The mice were trained three times daily for five days. The data from the last training session before the operation was used as the baseline. Mice were subjected to MCA for 2 h, followed by a series of neurological functional assessments on the 3d and 7d after reperfusion, including Bederson, mNSS, sticking test and corner test. All the mice receiving MCAO/R showed consistent neurological defects such as inability to bend the forelimb, rotation to the injured side and imbalance after operation. Compared with MCAO/R group, Wel and NBP could significantly reduce the Bederson, mNSS score, and the therapeutic effect on the 7d was better than that on the 3d (Figure 1D and E). Similarly, after 3d and 7d of treatment with Wel and NBP, the probability of turning to the injured side decreased significantly and in a dose-time dependent manner, and the time required to remove the sticker also exhibited the same trend (Figure 1F and G). Moreover, compared with MCAO/R group, mice treated with Wel and NBP gained weight (Figure 1C).

Wel Alleviated CI/RI in the MCAO/R Mice

As shown in Figure 2A–C, Wel and NBP treatment effectively reduced the infarction volumes and brain water content in a dose-dependent manner. LDH is a key indicator of the degree of cell damage. Therefore, the contents of LDH in brain tissue and serum of mice were detected. Compared with Sham group, the levels of LDH in MCAO/R group increased significantly. However, Wel and NBP could reverse the increase of LDH levels in different degrees, and the therapeutic effect of 7d was more significant than that of 3d (Figure 2D and E). HE staining showed that Wel and NBP groups could significantly reduced the pathological injury of brain tissue. Compared with MCAO/R group, the nuclear deformation and nuclear shrinkage of neurons in Wel and NBP groups were alleviated, and the degree of chromatin thickening was significantly reduced (Figure 2F and G). Nissl staining showed that in MCAO/R group, the staining of Nissl bodies became lighter, the number of Nissl bodies is decreased, the intercellular space is enlarged, and many vacuoles are formed. Compared with MCAO/R group, The trend of the decrease in the quantity of Nissl bodies in the Wel group and the NBP group was reversed, and they were arranged orderly, while the intercellular spaces and vacuoles were also reduced (Figure 2F and H). The above results indicated that Wel exhibits good potential against CI/RI neurological deficits.

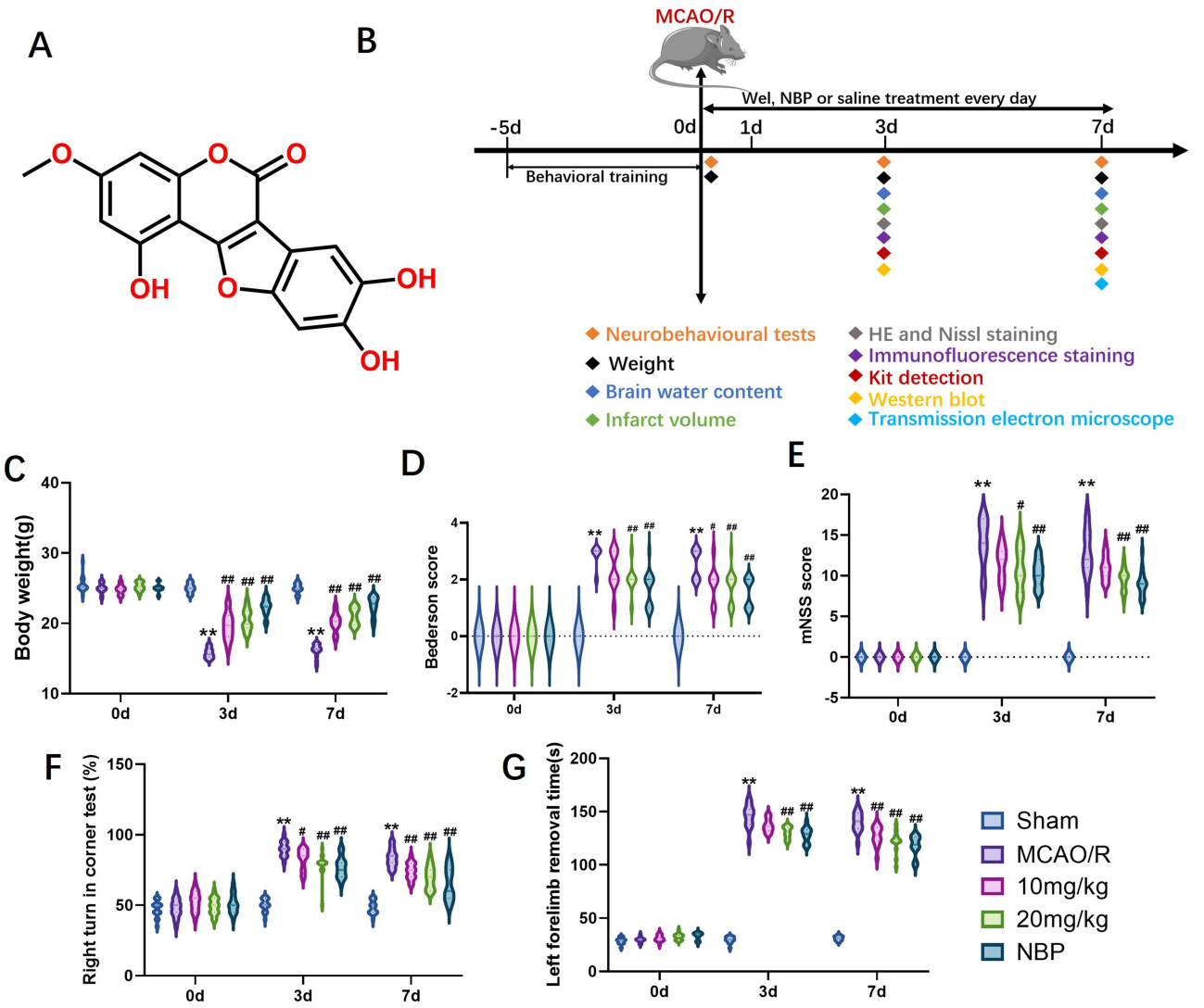

Figure 1 Wel improved neurological dysfunction after MCAO/R. (**A**) The chemical information of Wel. (**B**) Flow chart of the experiment. (**C**) Body weight was evaluated on the 0d, 3d and 7d. The neurological scores including Bederson score (**D**), mNSS score (**E**), Right turn in corner test (%) (**F**) and left forelimb removal time (**G**) were evaluated on the 0d, 3d and 7d. Data were expressed as mean ± SD (n=10-15). $^{**}P<0.01$ vs Sham; $^{\#\#}P<0.01$, $^{\#}P<0.05$ vs MCAO/R group. NBP: Butylphthalide.

Wel Inhibited Lipid Peroxidation and Ferroptosis in the MCAO/R Mice

When the brain suffers from CI/RI, the downregulated expression of GSH disrupts cellular iron metabolism, leading to the deposition of Fe^{2+} within cells and concurrently inducing a substantial accumulation of lipid peroxides (LPO, MDA, ROS).[32] As shown in Figure 3A and B, the content of Fe^{2+} in both brain tissue and serum were significantly elevated in the MCAO/R group, whereas a marked reduction was observed in the Wel group. These findings suggest that Wel may effectively alleviate iron overload. Iron overload could enhance lipid peroxidation, thereby giving rise to the occurrence of ferroptosis. The ultrastructural changes of neuronal mitochondria are the basic characteristics of cell ferroptosis.[33] Therefore, we observed the morphological changes of neurons and mitochondria by the transmission electron microscope. As shown in Figure 3C, in the Sham group, the neuronal morphology was regular, with a distinct outline, a clearly discernible nucleus, homogeneous chromatin, and the mitochondrial morphology was regular with intact and clearly visible cristae. Whereas in the neurons of the MCAO/R group, mitochondrial fragmentation occurs, cristae are reduced, and the mitochondrial membrane density was increased, which confirmed that CI/RI injury could induce ferroptosis to occur. Compared with Sham group, MCAO/R-treated neurons displayed fragmented mitochondria with decreased cristae

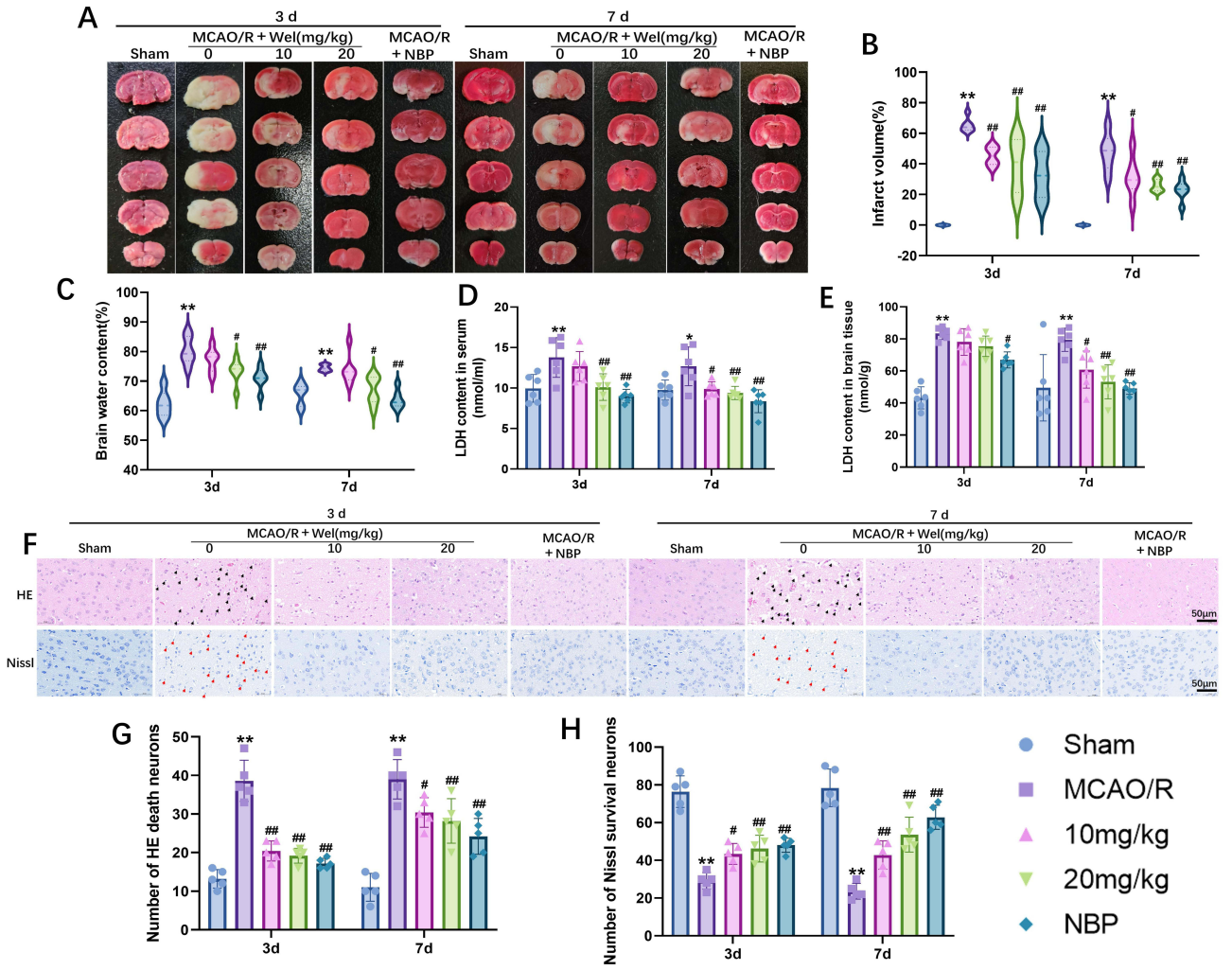

Figure 2 Wel alleviated CI/RI after MCAO/R. (**A**) TTC staining representative images. (**B** and **C**) The statistical analysis of brain infarct volume and brain water content (n=6). (**D** and **E**) The quantification of LDH levels in serum and brain tissue at 3d and 7d (n=6). (**F**) Representative H&E and Nissl staining cerebral slices were imaged by microscopy. The black arrow indicates that the outline of the cell is irregular, the nucleus shrinks, and cracks and vacuoles appear around the cell. The red arrow indicates that the Nissl staining color became lighter and vacuoles appear. (Scale bar:50μm). (**G** and **H**) Quantification of H&E and Nissl staining. Data were expressed as mean ± SD. $^{**}P<0.01$, $^{*}P<0.05$ vs Sham; $^{\#\#}P<0.01$, $^{\#}P<0.05$ vs MCAO/R group.

and increased mitochondrial membrane density, which confirmed that MCAO/R induces ferroptosis. However, Wel (20mg/kg) could conspicuously ameliorate this kind of injury. At the same time, the contents of MDA, GSH and LPO were detected. The level of MDA and LPO in MCAO/R group was significantly elevated, while the level of GSH was decreased. The Wel group could markedly reverse the damage (Figure 3D–I). When ferroptosis occurs in neurons, the X_C^- system is disordered, resulting in reduced GPX4 activity. As shown by Figure 3J and K immunofluorescence staining, the expression of GPX4 in MCAO/R group decreased significantly, while Wel increased the expression of GPX4 in different degrees. Similar results were obtained in the changes of GPX4 levels in brain tissue and serum. Wel could reverse the decrease of GPX4 level caused by MCAO/R (Figure 3L and M).

Wel Protected Against MCAO/R-Induced Ferroptosis in Mice Through Regulating the HIF-1α/SLC7A11/GPX4 Signaling Pathway

To further investigate the mechanism of Wel against ferroptosis, Western blot and immunofluorescence were employed to examine the influence of Wel on the activation of the HIF-1α signaling pathway in brain tissue. Research reveals that

https://doi.org/10.2147/DDDT.S528831

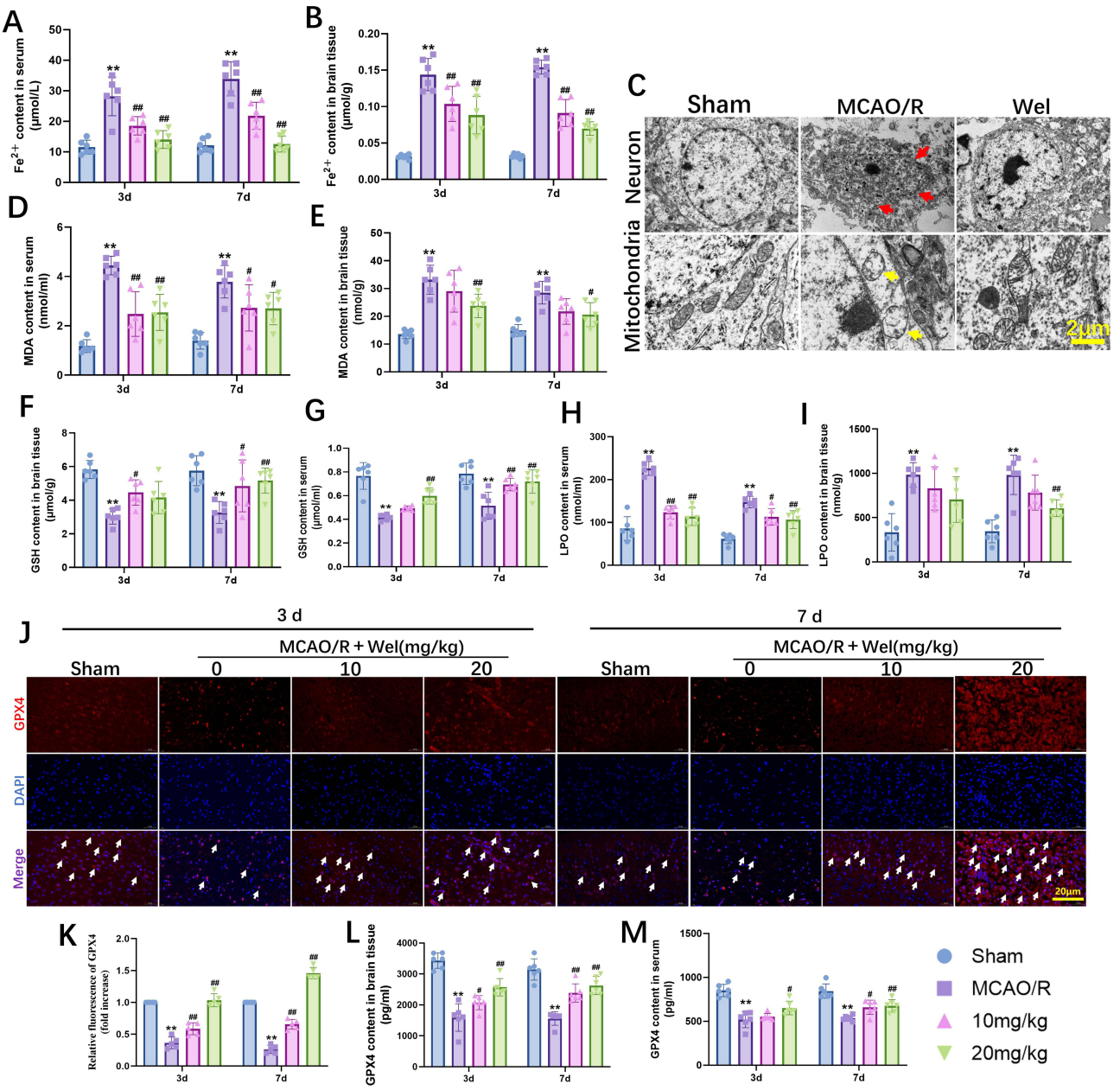

Figure 3 Wel inhibited lipid peroxidation and ferroptosis after MCAO/R. (**A** and **B**) The quantification of Fe^{2+}in serum and in brain tissue at 3d and 7d (n=6). (**C**) Representative TEM images of neurons and mitochondria in MCAO/R group and the Wel-treatment group. The red arrow indicates that the neurons with ruptured outline. The yellow arrow indicates that the mitochondria with decreased cristae (Scale bar: 2μm). (**D–I**) The quantification of MDA, GSH and LPO levels in serum and tissue brain at 3d and 7d (n=6). (**J** and **K**) Quantification of GPX4 fluorescence intensity (Scale bar: 20μm), the white arrows indicate the co-expression of GPX4 and DAPI. (**L–M**) The quantification of GPX4 in serum and brain tissue at 3d and 7d (n=6). Data were expressed as mean ± SD. $^{**}P<0.01$ vs Sham; $^{\#\#}P<0.01$, $^{\#}P<0.05$ vs MCAO/R group.

HIF-1α could regulate the level of SLC7A11. By double labeling with HIF-1α and SLC7A11, we found Wel increased the expression of HIF-1α/SLC7A11 in the brain of MCAO/R mice (Figure 4A–C). Similarly, the Wel also could significantly promoted the expression of HIF-1α, SLC7A11 and GPX4 protein (Figure 4D–G). These results further reveal that Wel may regulate ferroptosis through the HIF-1α/SLC7A11/GPX4 pathway.

 https://doi.org/10.2147/DDDT.S528831

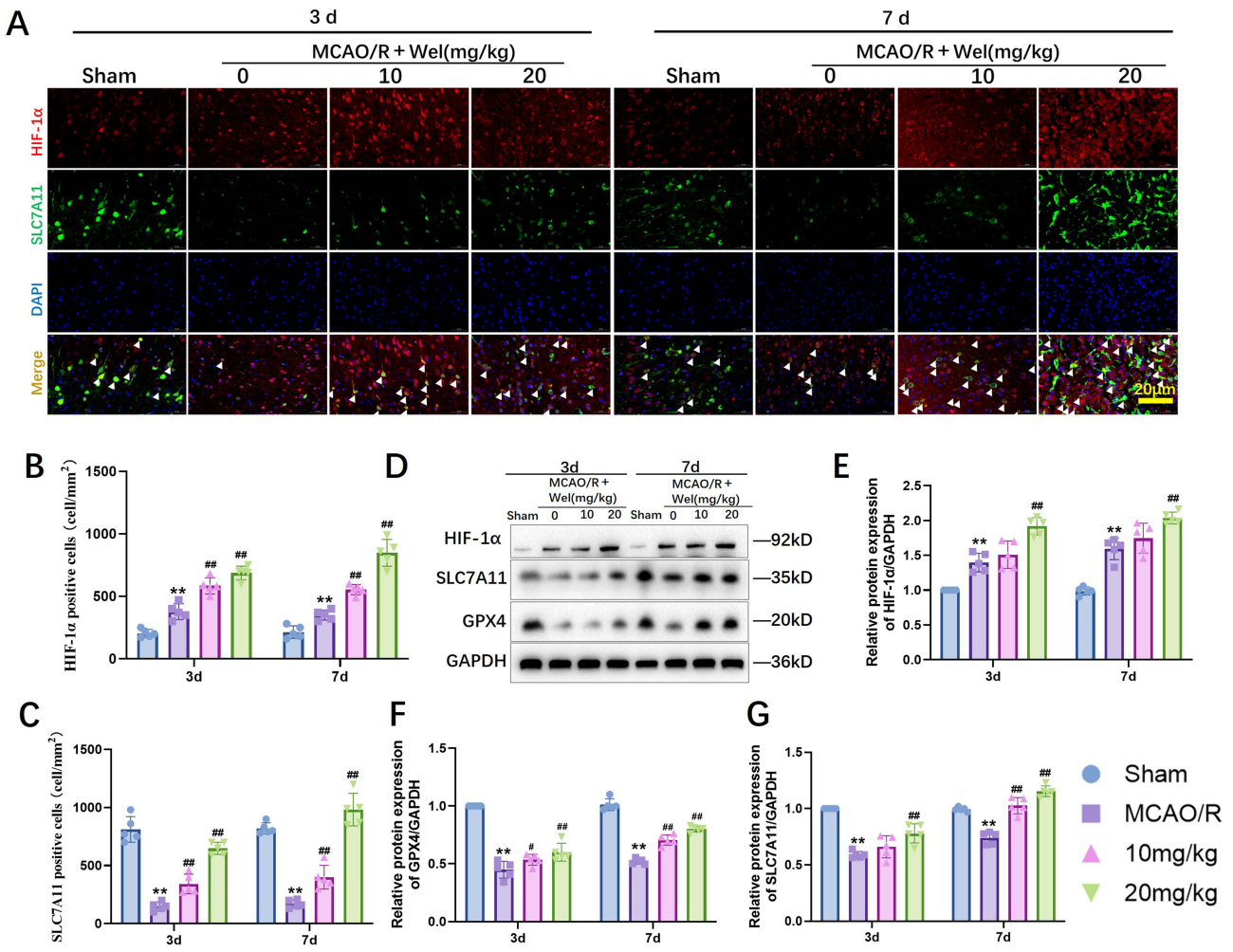

Figure 4 Wel inhibited ferroptosis after MCAO/R through regulating the HIF-1α/SLC7A11/GPX4 signaling pathway. (**A**) Representative images of the infarction area on 3d and 7d after Wel treatment contained with an antibody against HIF-1α (red) and SLC7A11 (green) by immunofluorescence (Scale bar: 20 μm), the white arrows indicate the co-expression of HIF-1α, SLC7A11 and DAPI. (**B** and **C**) Quantification of HIF-1α and SLC7A11 fluorescence intensity. (**D**–**G**) Representative bands and quantitative analysis of HIF-1α, SLC7A11 and GPX4 (n=5). Data were expressed as mean ± SD. $^{**}P<0.01$ vs Sham; $^{\#\#}P<0.01$, $^{\#}P<0.05$ vs MCAO/R group.

Wel Attenuated OGD/R-Induced Neuronal Injury in vitro

In order to simulate the effect of Wel on IS in vitro, PC12 cells were subjected to OGD/R treatment. First, we set a concentration gradient of Wel to treat PC12 cells and observed the changes in cell activity. The results showed that when the concentration of Wel reached 5 μM, the cell activity began to decline. When the concentration was more than 10 μM, the cell activity decreased significantly (Figure 5A). Therefore, we select the concentration of 0.625, 0.125 and 2.5 to start the next experiment. When the cells were subjected to OGD/R, the cell activity decreased significantly, and Wel could restore the cell activity in a dose-dependent manner, which was similar to that of NBP group (Figure 5B). We also detected the LDH level used cell lysate. The significant increased in the LDH level in the OGD/R group indicated the successful establishment of the model, while Wel and NBP could effectively reduce the release of LDH (Figure 5D). Meanwhile, we used Hoechst 33258 staining and an optical microscope to observe the changes in cell morphology and the degree of apoptosis. The results showed that in the OGD/R group, the nucleus shrunk and the refraction decreased, and the number of apoptotic cells increased. On the contrary, Wel and NBP can reverse cell damage and apoptosis (Figure 5C, E and F).

https://doi.org/10.2147/DDDT.S528831

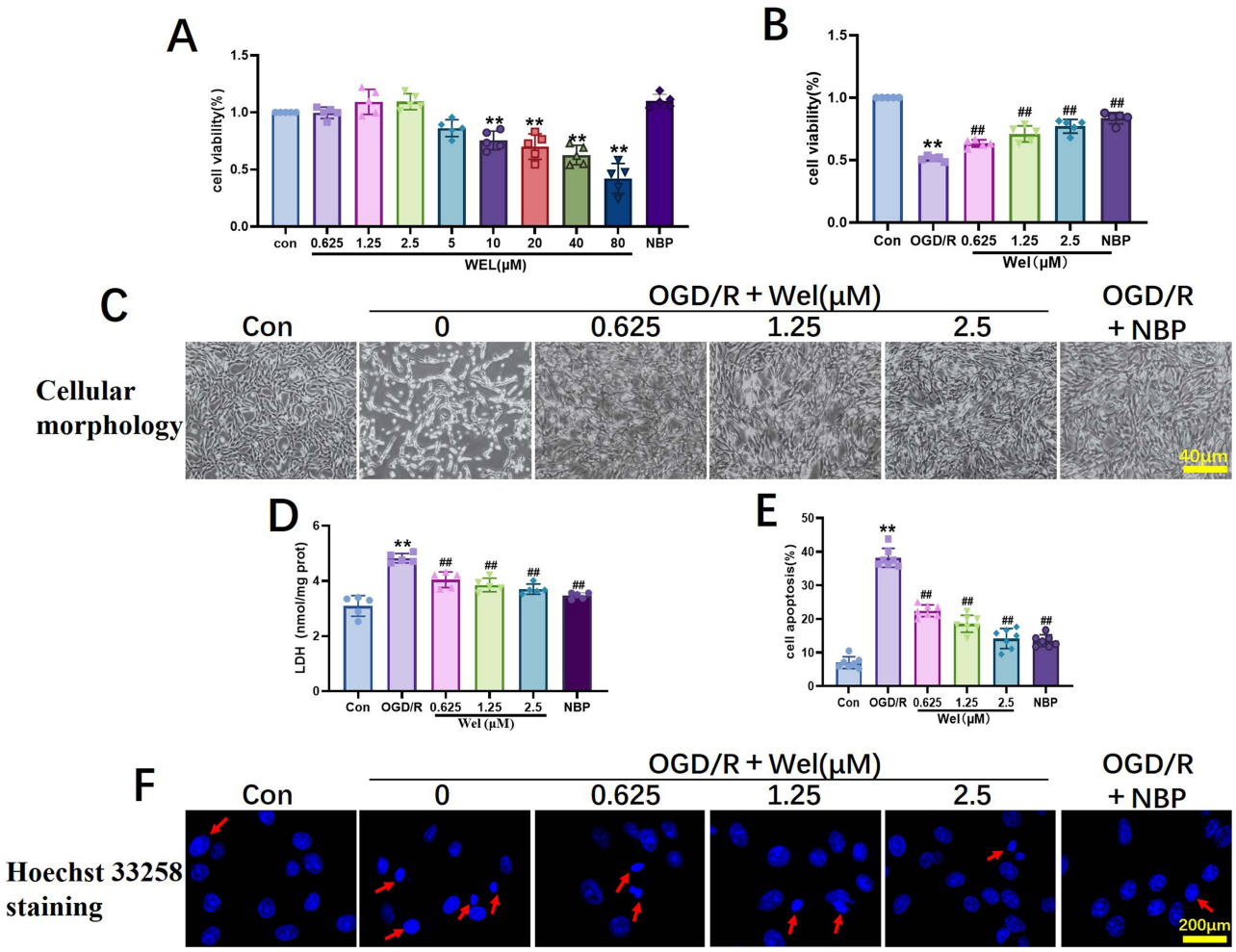

Figure 5 Wel attenuated OGD/R-induced neuronal injury in vitro. (**A** and **B**) Effects of Wel on viability of normal and OGD/R PC12 (n=5). (**C**) Effects of Wel on cell state of OGD/R PC12 (Scale bar: 40μm). (**D**) Quantification of LDH in PC12 cells (n=5) (**E** and **F**) Representative images and quantification of Wel on apoptosis of OGD/R PC12 (n=7, Scale bar: 200μm), the red arrows indicate apoptosis cells with nuclear shrunk. Data were expressed as mean ± SD. $^{**}P<0.01$ vs Con; $^{\#\#}P<0.01$ vs OGD/R group.

Wel Inhibited Lipid Peroxidation and Ferroptosis After OGD/R in vitro

To further verify the inhibitory effect of Wel on ferroptosis and lipid peroxidation, immunofluorescence was used to detect the accumulation of intracellular ROS (DHE) and the expression of Fe^{2+} (Ferro-Orange). As shown in Figure 6A–C and E, the fluorescence intensity of ROS and Fe^{2+} in the OGD/R group significantly increased, but gradually decreased with the increasing concentration of Wel, exhibiting a dose-dependent manner. At the same time, we further utilized the cell lysate to detect ferroptosis marker and lipid peroxides, including Fe^{2+}, GSH, LPO and MDA. The results were consistent with those of the in vivo experiments mentioned above. Wel decreased the contents of MDA, ROS, Fe^{2+} and LPO, while increasing the level of GSH (Figure 6D, F–H). These results suggested that Wel could enhance cellular antioxidation, reduce the accumulation of intracellular lipid peroxidation substrates, and thereby inhibit ferroptosis.

Wel Protected Against OGD/R-Induced Ferroptosis Through the HIF-1α/SLC7A11/GPX4 Signaling Pathway

Molecular docking plays a key role in drug design. Figure 7A shows the three-dimensional structure map of the binding of Wel and HIF-1α, which strongly binds to LEU188, ASP201, HIS199 and ARG238, indicating that Wel may have the ability to regulate HIF-1α. Then, we detected the level of HIF-1α, SLC7A11 and GPX4 proteins in the cell lysate by

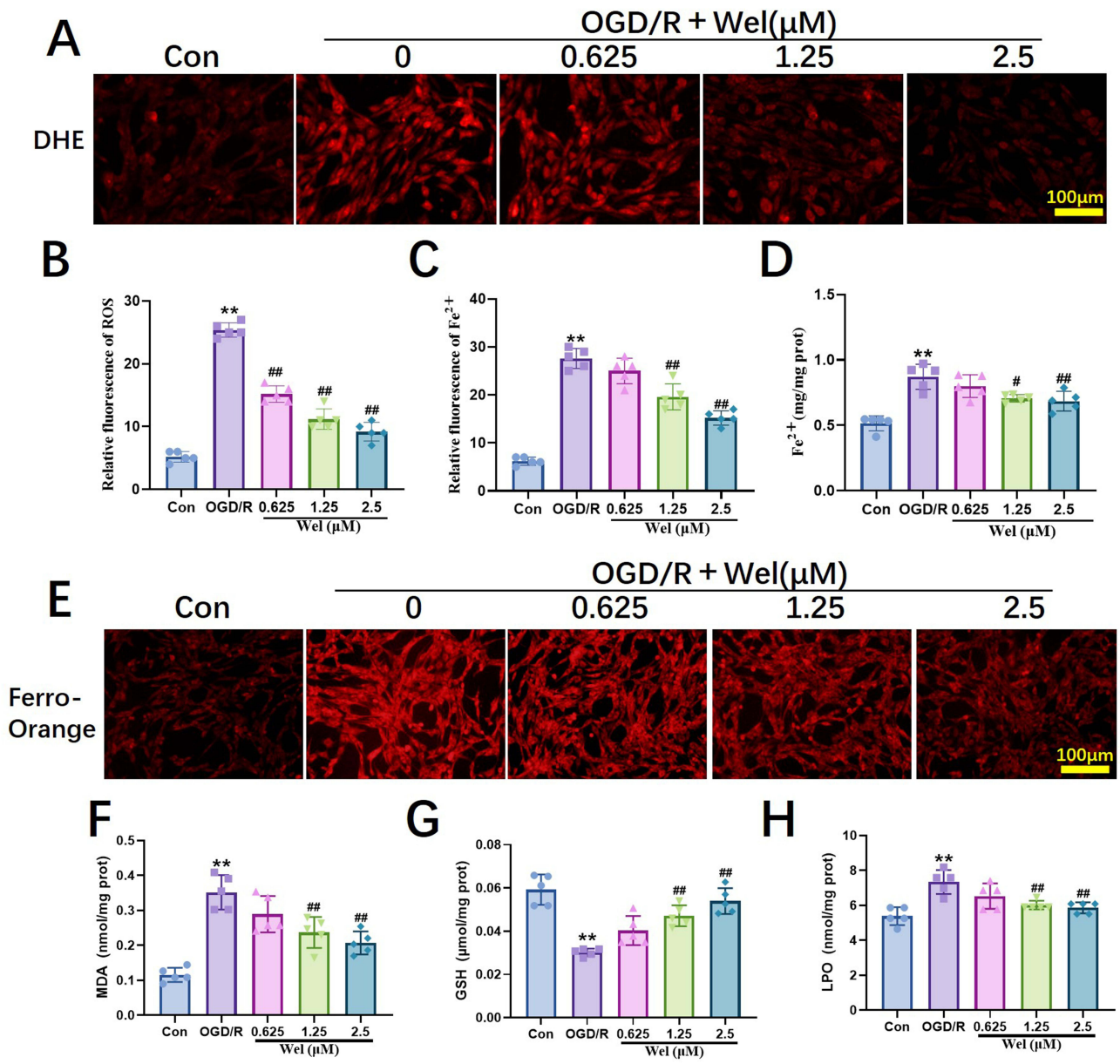

Figure 6 Wel inhibited lipid peroxidation and ferroptosis after OGD/R in vitro. (**A** and **B**) Representative images and quantification of the level of ROS by DHE staining in PC12 cells (n=5, Scale bar: 100μm). (**C**) Quantification of the Fe^{2+} fluorescence intensity by Ferro-Orange staining in PC12 cells. (**D**) Quantification of Fe^{2+}in PC12 cells (n=5). (**E**) Representative images of the level of the Fe^{2+} fluorescence intensity by Ferro-Orange staining in PC12 cells. (**F**–**H**) Quantification of MDA, GSH and LPO in PC12 cells (n=5). Data were expressed as mean ± SD. $^{**}P<0.01$ vs Con; $^{\#\#}P<0.01$, $^{\#}P<0.05$ vs OGD/R group.

Western blot analysis. The trend was consistent with the in vivo experimental results. Wel significantly elevated the level of HIF-1α protein, thereby enhancing the expression of SLC7A11 and GPX4 protein (Figure 7B–E). Interestingly, we observed that the expression of HIF-1α in OGD/R-treated PC12 cells was upregulated, and this increase was more pronounced following Wel intervention. This phenomenon might be attributed to the cellular stress response elicited for self-protection after ischemia and hypoxia exposure.

https://doi.org/10.2147/DDDT.S528831

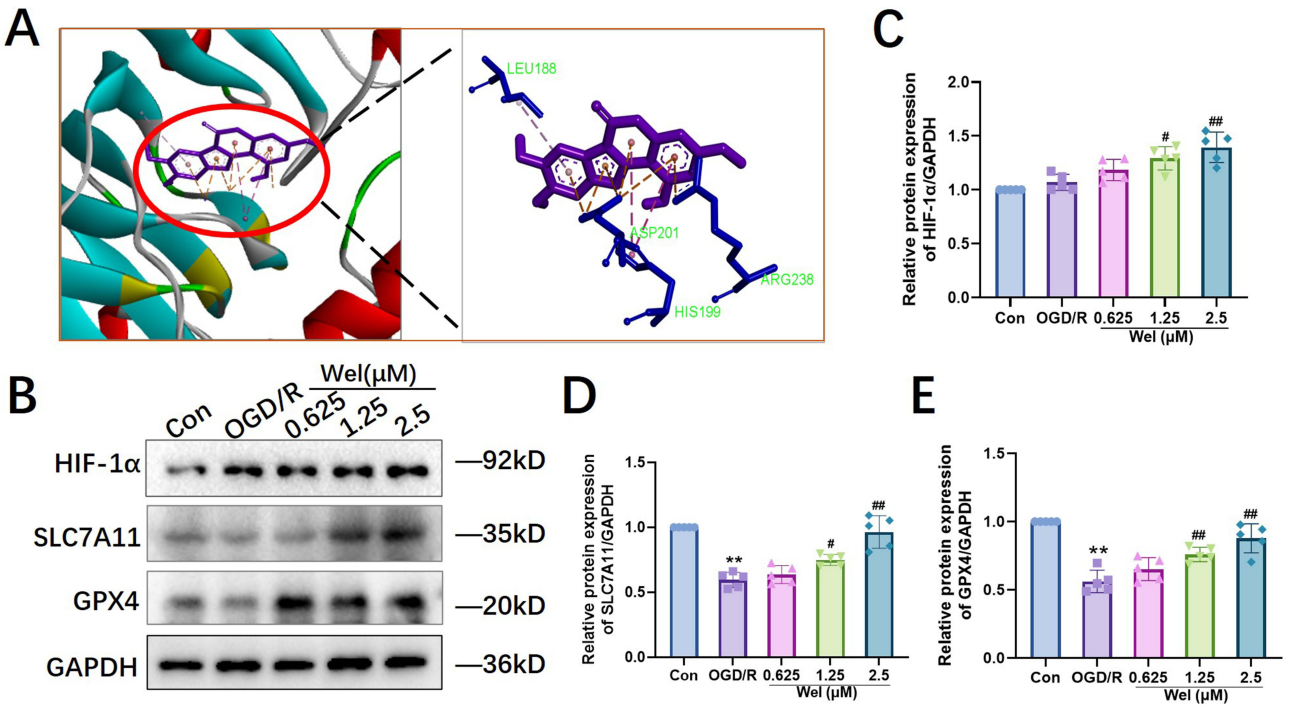

Figure 7 Wel protected against OGD/R-induced ferroptosis through the HIF-1α/SLC7A11/GPX4 signaling pathway. (**A**) Three-dimensional docking structure diagram of HIF-1α and Wel. (**B**–**E**) Representative bands and quantitative analysis of HIF-1α, SLC7A11 and GPX4 (n=5). Data were expressed as mean ± SD. $^{**}P<0.01$ vs Con; $^{\#\#}P<0.01$, $^{\#}P<0.05$ vs OGD/R group.

Wel Inhibited OGD/R-Induced Ferroptosis Through Knockdown of HIF-1α

To explore the role of HIF-1α in the Wel-inhibited ferroptosis function, the expression of HIF-1α in cells was downregulated by siRNA transfection. Western blot analysis and qRT-PCR were used to detect the expression of HIF-1α and downstream related genes and proteins in cell lysate. As shown in Figure 8A–C, the mRNA and protein levels of HIF-1α siRNA-3 decreased most significantly compared with Scrb group. Therefore, HIF-1α siRNA-3 was selected for the subsequent experiment. Western blot results showed that in OGD/R-treated PC12 cells, knockdown of HIF-1α weakened Wel's role in increasing the expression of the SLC7A11 and GPX4 proteins (Figure 8D–F). In addition, these results proved that HIF-1α knockdown remarkably reversed the inhibitory effects of Wel on Fe^{2+} content and cell apoptosis, and reversed the enhancement effect of Wel on cell viability (Figure 8G–J). All the results indicated that inhibition of HIF-1α abolish the therapeutic effect of Wel in PC12 cells.

Discussion

IS is a major disease that endangers human health. Currently, the treatment mainly relies on thrombolysis therapy, but it often leads to secondary ischemic reperfusion injury. Consequently, there is an urgent need to develop effective neuroprotectants to alleviate ischemic reperfusion injury.[34] The preventive and therapeutic efficacy of traditional Chinese medicine and natural products in cardiovascular and cerebrovascular diseases has increasingly drawn substantial attention.[35] Wel is a furanocoumarin compound extracted from the medicinal plant *Eclipta prostrata L*. Research revealed that Wel could reduce the inflammatory response in the hippocampal region of rats, indicating potential neuroprotective effects.[19,20] Yang et al preliminarily verified that Wel inhibited OGD/R-induced ferroptosis by mediating GPX4 expression.[21] Furthermore, prior studies have indicated that Wel inhibits ferroptosis through the Nrf2/HO-1 signaling pathway, thereby alleviating lung and liver injuries.[16,17] However, limited information was available regarding whether Wel could enhance the neurological function of mice following stroke and its underlying mechanism of action.

Our study was the first to demonstrate that Wel could exert significant neuroprotective effects against CI/RI both in vivo and in vitro. Specifically, Wel markedly reduced cerebral infarct volume and brain swelling, lowered the Bederson and mNSS

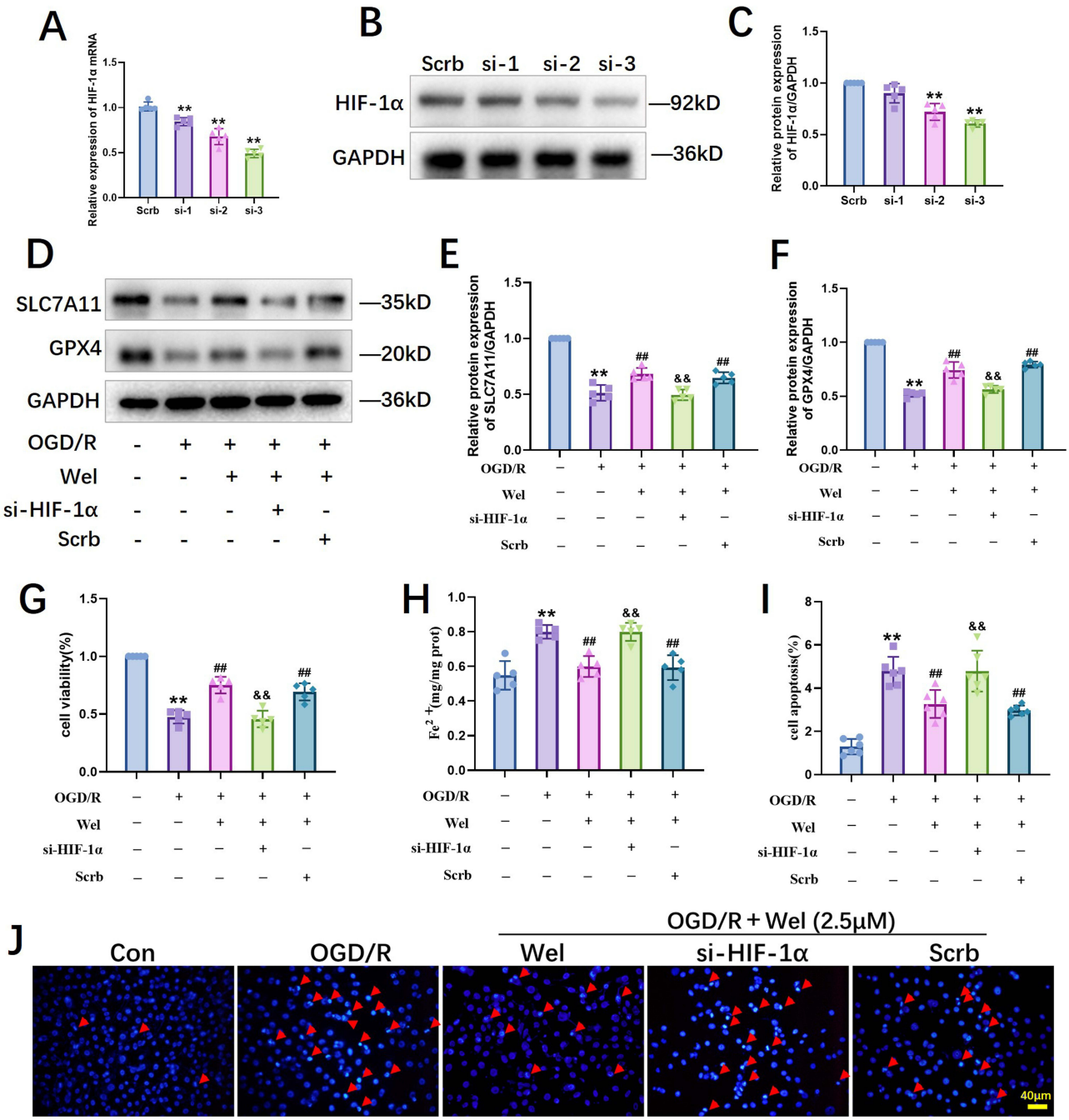

Figure 8 Wel inhibits OGD/R-induced ferroptosis through knockdown of HIF-1α. (**A**) Efficiency of HIF-1α silence by siRNA was analyzed by qRT-PCR (n=5). (**B** and **C**) Efficiency of HIF-1αsilence by siRNA was analyzed by Western blot (n=5). (**D**–**F**) Representative bands and quantitative analysis of SLC7A11 and GPX4 (n=5). (**G**) The cell viability was measured by CCK-8 kits (n=5). (**H**) The content of Fe^{2+} was measured by assay kit (n=5). (**I** and **J**) The Hoechst 33258 staining and quantification of cell apoptosis (n=6, Scale bar: 40μm), the red arrows indicate apoptotic cells with nuclear shrunk. Data were expressed as mean ± SD. $^{**}P<0.01$ vs Con; $^{\#\#}P<0.01$, vs OGD/R; $^{\&\&}P<0.01$ vs OGD/R^{+}Wel group.

scores in mice, decreased the likelihood of turning toward the right side, shortened the time required to remove the sticky label, and restored neurological function. These findings were further corroborated by HE and Nissl staining, which revealed that Wel mitigated neuronal nuclear shrinkage and reduced damage to Nissl bodies. LDH is highly expressed in the cytoplasm of neuronal cells. Following cellular damage induced by cerebral ischemia, LDH is released into the extracellular space, subsequently diffusing into the cerebrospinal fluid and traversing the compromised blood-brain barrier to enter the blood-stream and brain tissue. This results in a rapid elevation of LDH levels in serum and brain tissue. Consequently, the

https://doi.org/10.2147/DDDT.S528831

measurement of LDH can serve as an important indicator of the extent of IS.[36] Hence, we detected the LDH levels in vivo and in vitro. It was observed that CI/RI injury led to the accumulation of LDH, whereas Wel mitigated this damage. Moreover, at the cellular level, our findings demonstrated that Wel significantly suppressed OGD/R-induced neuronal apoptosis. These results suggest that Wel may be considered a potential and effective therapeutic candidate for IS.

When the brain undergoes ischemic injury, mitochondrial respiratory chain dysfunction occurs, resulting in a significant accumulation of ROS in the brain.[37] The immunofluorescence analysis in vitro verified that the Wel significantly attenuated ROS levels. ROS can directly oxidize polyunsaturated fatty acids (PUFAs) on the cell membrane, thereby initiating LPO chain reactions. LPO refers to lipid peroxides formed through the action of free radicals or reactive oxygen species on unsaturated fatty acids. When LPO acts on specific PUFAs, MDA is generated via β-cleavage reactions.[38] MDA is the primary product of LPO and serves as a critical biomarker for lipid oxidative damage in biological systems.[12] Therefore, we quantified the levels of lipid peroxidation markers, including ROS, LPO, and MDA. The results showed that ROS, LPO and MDA levels were significantly increased in the CI/RI group, leading to damage in cell membrane structure and function. Following Wel treatment, the levels of these lipid peroxidation markers were substantially reduced. Glutathione (GSH), a key non-enzymatic antioxidant, serves as a substrate for GSH peroxidase, thereby inhibiting lipid peroxidation, protecting cell membranes, and restoring cellular function.[39] Our findings revealed that Wel could reverse the CI/RI-induced reduction in GSH levels, indicating its potential to mitigated lipid peroxidation damage following IS.

Mitochondria serve as the primary sites for the synthesis of iron-sulfur clusters and heme, processes that necessitate the involvement of iron ions. Under pathological conditions, mitochondrial dysfunction and energy metabolism disorders result in iron overload, exacerbating the vicious cycle of lipid peroxidation and ferroptosis.[40] Hence, in this study, the morphological changes of neuronal mitochondria in mouse brain tissue were observed. The CI/RI-induced damage led to significant mitochondrial membrane rupture, a reduction in mitochondrial count, and the disappearance of cristae. Notably, Wel treatment was found to ameliorate mitochondrial morphology. Furthermore, we quantified Fe^{2+} levels and demonstrated that Wel effectively suppressed Fe^{2+} accumulation induced by CI/RI. At the same time, Ferro-orange staining in vitro experiments revealed that Wel significantly diminished Fe^{2+} fluorescence intensity. Collectively, these results strongly indicated that Wel mitigates the accumulation of lipid reactive oxygen species, enhances cellular antioxidant capacity, repairs mitochondrial damage, and inhibits ferroptosis following CI/RI injury. Nevertheless, the precise mechanisms underlying Wel's protective effects against CI/RI-induced damage remain to be elucidated.

Recombinant solute carrier family 7, member 11 (SLC7A11) serves as the catalytic subunit of cell membrane transporter system X_C^-. Its upregulation enhances intracellular cysteine levels, thereby promoting GSH synthesis and enhancing the activity of GPX4. This protective mechanism safeguards neurons against ferroptosis induced by cerebral ischemia.[41,42] HIF-1α, a heterodimeric transcription factor composed of α and β subunits, regulates downstream proteins such as SLC7A11 and GPX4, which play critical roles in modulating oxidative stress, inflammation, and cell death. Under normal oxygen conditions, HIF-1α is rapidly degraded through the ubiquitin-proteasome pathway. During cerebral ischemia and hypoxia, the activity of PHDs is inhibited, thereby blocking the PHD-VHL-proteasome pathway that mediates the degradation of HIF-1α. This leads to the accumulation and nuclear translocation of HIF-1α. Upon binding to the hypoxia response element (HRE), HIF-1α induces alterations in the expression of downstream target genes.[43] Studies have already demonstrated that HIF-1α plays a critical role in SLC7A11 protein expression in rat brains, whereas overexpression of HIF-1α enhances the expression of SLC7A11 protein in hepatocytes.[14,44] In this study, we observed a phenomenon consistent with previous reports, that is, both HIF-1α fluorescence and protein expression were significantly increased in the CI/RI model group. Interestingly, Wel was found to further enhance the level of HIF-1α in a dose-time-effect dependent manner. As a critical factor regulating the human body's response to hypoxia, HIF-1α is either minimally expressed or not detectable under physiological conditions. Upon exposure of cells to ischemia and hypoxia, a self-protective stress response occurs (ie, an increase in HIF-1α), which regulates cellular energy metabolism, apoptosis, and other processes to adapt to the hypoxic environment and mitigate ischemic and hypoxic damage.[9,45] However, this upregulation alone is insufficient for sustaining autonomous cellular repair. Notably, upon treatment with Wel, the level of HIF-1α protein is further elevated, thereby enhancing the repair of cellular damage.

In view of the direct regulatory of Wel on HIF-1α, we have also demonstrated this point via molecular docking technology. Specifically, Wel can form a stable complex with the protein crystal structure of HIF-1α through four binding sites, namely LEU188, ASP201, HIS199, and ARG238. In addition, Wel has been shown to enhance the fluorescence co-

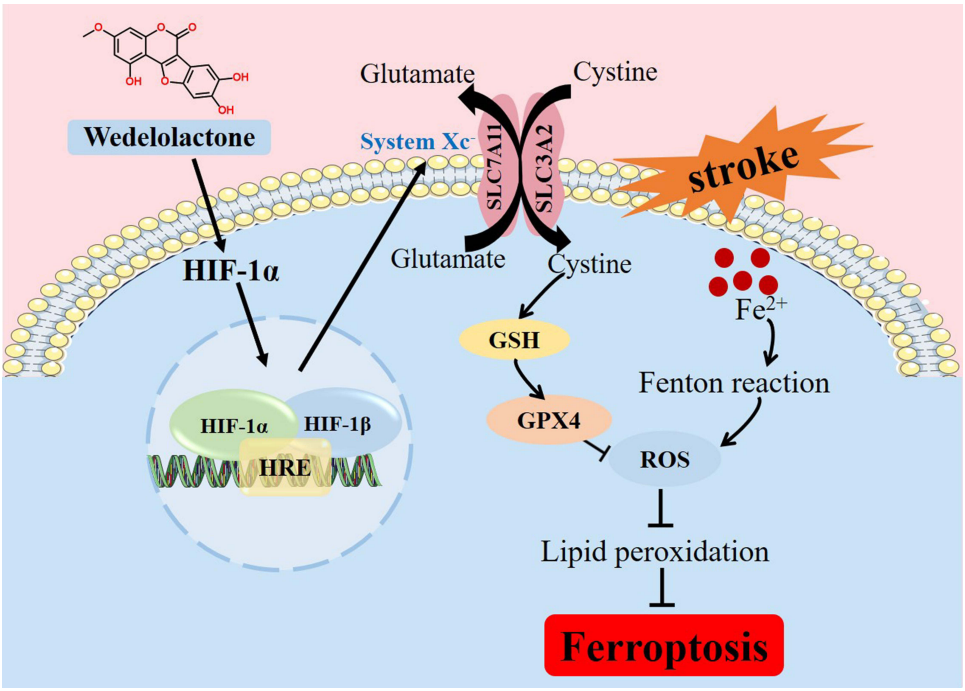

Figure 9 Schematic overview of the mechanism underlying the protective effects of Wel against cerebral ischemia/reperfusion injury (CI/RI)-induce ferroptosis.

expression of HIF-1α and SLC7A11 in MCAO/R mice, as well as increase the levels of HIF-1α and SLC7A11 proteins. These results also confirmed the previously reported conclusion that HIF-1α directly regulate SLC7A11 to exert its biological functions. GPX4 is a critical enzyme responsible for scavenging lipid peroxides. In the presence of GSH, it catalyzes the conversion of GSH into oxidized glutathione while reducing toxic lipid peroxides to non-toxic lipid alcohols, thereby preventing ferroptosis.[46] Studies have demonstrated that mice that the absence of SLC7A11 or GPX4 proteins in mice induces ferroptosis in cells, leading to cognitive dysfunction and neurodegenerative damage.[6,47] Therefore, we detected GPX4 levels both in vivo and in vitro using assay kit. Immunofluorescence labeling revealed a decrease in GPX4 content and fluorescence intensity in the MCAO/R group, which was reversed by Wel treatment. Consistently, Western blot analysis confirmed this trend. Furthermore, cell transfection experiments indicated that Wel mitigates CI/RI damage at least partially through the regulation of HIF-1α. These results suggested that Wel may alleviate ferroptosis following CI/RI by reducing iron overload, reducing mitochondrial ROS production and lipid peroxidation. This effect is likely mediated through the regulation of the HIF-1α/SLC7A11/GPX4 signaling pathway.

Although this study clarified the therapeutic effects of Wel on CI/RI injury and its potential mechanism of action, certain limitations should be acknowledged. Firstly, the study did not include verification of Wel's regulatory effect on HIF-1α using gene knockout mice. It remains unclear whether other potential pathways beyond HIF-1α are involved in Wel's mechanism. Moreover, no comparison was conducted between Wel and iron chelators. Consequently, it could only be preliminarily demonstrated that Wel holds potential for mitigating CI/RI injury, potentially through the HIF-1α-mediated ferroptosis pathway. Secondly, the PC12 cell line was used at the cellular level in this study. Further research will be conducted in primary neuronal cells to confirm our findings. Thirdly, it is essential to further evaluate the long-term efficacy of Wel after CI/RI. The disparities between animal models and human disease development must be acknowledged. Therefore, conducting real-world studies to assess the clinical impact of Wel on functional recovery in both male and female patients with CI/RI is warranted. Fourthly, despite previous studies have examined the pharmacokinetic characteristics of Wel in rats, which demonstrated moderate absorption and significant tissue distribution potentially constrained by its relatively low water solubility, it remains imperative to evaluate the pharmacokinetics and safety of Wel in humans as the next step. Furthermore, enhancing its bioavailability and expanding its clinical applicability can be effectively achieved through the development of more soluble derivatives or by formulating it as nanoparticles or liposomes. This direction presents both opportunities and challenges for us and other researchers.

Conclusions

To summarize, our research results revealed that Wel could remarkably reduce the cerebral infarction volume and brain swelling, and repair neurological function. Wel exerts its protective effect against CI/RI by activating HIF-1α/SLC7A11/GPX4 signal pathway at least in part to inhibit ferroptosis in neurons (Figure 9). Future research will continue to evaluate the long-term efficacy of Wel after CI/RI. Additionally, further pharmacokinetic and safety evaluations of Wel in humans will be conducted to enhance its clinical translation and applicability.

Data Sharing Statement

The data used to support the findings of this study are available from the corresponding authors upon request.

Ethical Approval

The protocol for the animal study was reviewed and approved by the Institutional Animal Ethical Committee of Fourth Military Medical University (Shaanxi, China).

Author Contributions

All authors made a significant contribution to the work reported, whether that is in the conception, study design, execution, acquisition of data, analysis and interpretation, or in all these areas; took part in drafting, revising or critically reviewing the article; gave final approval of the version to be published; have agreed on the journal to which the article has been submitted; and agree to be accountable for all aspects of the work.

Funding

This work was financially supported by the National Natural Science Foundation of China (No. 82405134), the Clinical Medicine and Pharmacy Research Center, Air Force Medical University (LHJJ2024-YX03, LHJJ2024-YX21), and the project for enhancing medical staff training of Xijing Hospital (XJZT24CZ14, XJZT24QN55).

Disclosure

The authors declare that they have no known competing financial interests or personal relationships that could have appeared to influence the work reported in this paper.

References

1. Martin SS, Aday AW, Almarzooq ZI, et al. Heart-disease and stroke statistics: a report of us and global data from the American heart association. *Circulation*. 2024;149(8):e347–e913. doi:10.1161/CIR.0000000000001209
2. Widimsky P, Snyder K, Sulzenko J, et al. Acute ischaemic stroke: recent advances in reperfusion treatment. *Eur Heart J*. 2023;44(14):1205–1215. doi:10.1093/eurheartj/ehac684
3. Campbell BCV, De Silva DA, Macleod MR, et al. Ischaemic stroke. *Nat Rev Dis Primers*. 2019;5(1):70. doi:10.1038/s41572-019-0118-8
4. Newton K, Strasser A, Kayagaki N, et al. Cell death. *Cell*. 2024;187(2):235–256. doi:10.1016/j.cell.2023.11.044
5. Pope LE, Dixon SJ. Regulation of ferroptosis by lipid metabolism. *Trends Cell Biol*. 2023;33(12):1077–1087. doi:10.1016/j.tcb.2023.05.003
6. Koppula P, Zhuang L, Gan B. Cystine transporter SLC7A11/xCT in cancer: ferroptosis, nutrient dependency, and cancer therapy. *Protein Cell*. 2021;12(8):599–620. doi:10.1007/s13238-020-00789-5
7. Xie Y, Kang R, Klionsky DJ, et al. GPX4 in cell death, autophagy, and disease. *Autophagy*. 2023;19(10):2621–2638. doi:10.1080/15548627.2023.2218764
8. Li X, Jankovic J, Le W. Iron chelation and neuroprotection in neurodegenerative diseases. *J Neural Transm*. 2021;118(3):473–477. doi:10.1007/s00702-010-0518-0
9. Vatte S, Ugale R. HIF-1, an important regulator in potential new therapeutic approaches to ischemic stroke. *Neurochem Int*. 2023;170:105605. doi:10.1016/j.neuint.2023.105605
10. Li X, Li L, Lei W, et al. Young rat vascular endothelial cells promote neurological recovery of stroke aged rat via HIF-1α. *iScience*. 2025;28(6):112552. doi:10.1016/j.isci.2025.112552
11. Kang P, Zhou X, Zhao S, et al. Inhibitors of p53 apoptosis-stimulating protein mitigate acute kidney injury by modulating the HIF −1α/ SLC7A11 pathway to suppress ferroptosis. *J Cell Mol Med*. 2025;29(11):e70580. doi:10.1111/jcmm.70580
12. Ju L, Diao J, Zhang J, et al. Shenshuai Yingyang Jiaonang ameliorates chronic kidney disease-associated muscle atrophy in rats by inhibiting ferroptosis mediated by the HIF-1α/SLC7A11 pathway. *Heliyon*. 2024;10(8):e29093. doi:10.1016/j.heliyon.2024.e29093
13. Yuan S, Wei C, Liu G, et al. Sorafenib attenuates liver fibrosis by triggering hepatic stellate cell ferroptosis via HIF-1α/SLC7A11 pathway. *Cell Prolif*. 2022;55(1):e13158. doi:10.1111/cpr.13158

14. Sims B, Clarke M, Francillion L, et al. Hypoxic preconditioning involves system Xc^- regulation in mouse neural stem cells. *Stem Cell Res*. 2012;8(2):285–291. doi:10.1016/j.scr.2011.09.002
15. Feng L, Zhai YY, Xu J, et al. A review on traditional uses, phytochemistry and pharmacology of Eclipta prostrata (L.) L. *J Ethnopharmacol*. 2019;245:112109. doi:10.1016/j.jep.2019.112109
16. Fan R, Sui J, Dong X, et al. Wedelolactone alleviates acute pancreatitis and associated lung injury via GPX4 mediated suppression of pyroptosis and ferroptosis. *Free Radic Biol Med*. 2021;173:29–40. doi:10.1016/j.freeradbiomed.2021.07.009
17. Yin Y, Mu F, Zhang L, et al. Wedelolactone activates the PI3K/AKT/NRF2 and SLC7A11/GPX4 signalling pathways to alleviate oxidative stress and ferroptosis and improve sepsis-induced liver injury. *J Ethnopharmacol*. 2025;344:119557. doi:10.1016/j.jep.2025.119557
18. Chen Q, Wu X, Gao X, Song H, Zhu X. Development and validation of an ultra-performance liquid chromatography method for the determination of wedelolactone in rat plasma and its application in a pharmacokinetic study. *Molecules*. 2019;24(4):762. doi:10.3390/molecules24040762
19. Wei J, Wang Y, Wang X, et al. Rapid screening of active ingredients and action mechanisms of Ecliptae Herba for treating Alzheimer's disease by UPLC-Q-TOF/MS and "component-target-pathway" network. *Fitoterapia*. 2023;169:105613. doi:10.1016/j.fitote.2023.105613
20. Muke S, Kaikini A, Peshattiwar V, et al. Neuroprotective effect of coumarin nasal formulation: kindling model assessment of epilepsy. *Front Pharmacol*. 2018;9:992. doi:10.3389/fphar.2018.00992
21. Yang H, Liu D, Wang Y. Wedelolactone attenuates cerebral ischemia-reperfusion injury by blocking GPX4-mediated ferroptosis. *J Men Health*. 2023;19(10):120–126.
22. Tao X, Liu K, Li W, et al. Saponin of Aralia taibaiensis promotes angiogenesis through VEGF/VEGFR2 signaling pathway in cerebral ischemic mice. *J Ethnopharmacol*. 2023;317:116771. doi:10.1016/j.jep.2023.116771
23. Zhang W, Gao K, Bai Y, et al. Wedelolactone attenuates liver fibrosis and hepatic stellate cell activation by suppressing the hippo pathway. *Rejuvenation Res*. 2024;27(6):207–219. doi:10.1089/rej.2024.0053
24. Lourbopoulos A, Karacostas D, Artemis N, et al. Effectiveness of a new modified intraluminal suture for temporary middle cerebral artery occlusion in rats of various weight. *J Neurosci Methods*. 2008;173(2):225–234. doi:10.1016/j.jneumeth.2008.06.018
25. Zhao B, Zhang S, Amin N, et al. Thymoquinone regulates microglial M1/M2 polarization after cerebral ischemia-reperfusion injury via the TLR4 signaling pathway. *Neurotoxicology*. 2024;101:54–67. doi:10.1016/j.neuro.2024.02.002
26. Liu C, Liu K, Tao X, et al. Pharmacodynamics and mechanism of *Erigeron breviscapus* granules in the treatment of ischemic stroke in mice by regulating sphingolipid metabolism based on metabolomics. *J Pharm Biomed Anal*. 2024;242:116058. doi:10.1016/j.jpba.2024.116058
27. Wang K, Zhao H, Chen J, et al. Toona sinensis fruit polyphenols alleviate cerebral ischemia-reperfusion injury in rats by inhibiting MAPK signaling pathways and NLRP3 inflammasome/pyroptosis. *J Ethnopharmacol*. 2025;342:119375. doi:10.1016/j.jep.2025.119375
28. Liao YC, Wang JW, Guo C, et al. *Cistanche tubulosa* alleviates ischemic stroke-induced blood-brain barrier damage by modulating microglia-mediated neuroinflammation. *J Ethnopharmacol*. 2023;309:116269. doi:10.1016/j.jep.2023.116269
29. Chen N, Zhou Z, Li J, et al. 3-n-butylphthalide exerts neuroprotective effects by enhancing anti-oxidation and attenuating mitochondrial dysfunction in an in vitro model of ischemic stroke. *Drug Des Devel Ther*. 2018;12:4261–4271. doi:10.2147/DDDT.S189472
30. Kim S, Chen J, Cheng T, et al. PubChem 2025 update. *Nucleic Acids Res*. 2025;53(D1):D1516–D1525. doi:10.1093/nar/gkae1059
31. Berman H, Henrick K, Nakamura H. Announcing the worldwide protein data bank. *Nat Struct Biol*. 2003;10(12):980. doi:10.1038/nsb1203-980
32. Hu X, Bao Y, Li M, et al. The role of ferroptosis and its mechanism in ischemic stroke. *Exp Neurol*. 2024;372:114630. doi:10.1016/j.expneurol.2023.114630
33. Pan F, Xu W, Ding J, et al. Elucidating the progress and impact of ferroptosis in hemorrhagic stroke. *Front Cell Neurosci*. 2023;16:1067570. doi:10.3389/fncel.2022.1067570
34. Xi ZC, Ren HG, Ai L, et al. Ginsenoside Rg1 mitigates cerebral ischaemia/reperfusion injury in mice by inhibiting autophagy through activation of mTOR signalling. *Acta Pharmacol Sin*. 2024;45(12):2474–2486. doi:10.1038/s41401-024-01334-4
35. Zhang W, Zhang P, Xu LH, et al. Ethanol extract of Verbena officinalis alleviates MCAO-induced ischaemic stroke by inhibiting IL17A pathway-regulated neuroinflammation. *Phytomedicine*. 2024;123:155237. doi:10.1016/j.phymed.2023.155237
36. Li X, Tian X. The protective effects of Pimavanserin against cerebral ischemia-induced brain injury. *Bioengineered*. 2021;12(1):7481–7494. doi:10.1080/21655979.2021.1978617
37. Kim S, Lee W, Jo H, et al. The antioxidant enzyme Peroxiredoxin-1 controls stroke-associated microglia against acute ischemic stroke. *Redox Biol*. 2022;54:102347. doi:10.1016/j.redox.2022.102347
38. Gebicki JM. Oxidative stress, free radicals and protein peroxides. *Arch Biochem Biophys*. 2016;595:33–39. doi:10.1016/j.abb.2015.10.021
39. Liu Y, Wang Y, Mi Y, et al. Loureirin C inhibits ferroptosis after cerebral ischemia reperfusion through regulation of the Nrf2 pathway in mice. *Phytomedicine*. 2023;113:154729. doi:10.1016/j.phymed.2023.154729
40. Xiao P, Huang H, Zhao H, et al. Edaravone dexborneol protects against cerebral ischemia/reperfusion-induced blood-brain barrier damage by inhibiting ferroptosis via activation of nrf-2/HO-1/GPX4 signaling. *Free Radic Biol Med*. 2024;217:116–125. doi:10.1016/j.freeradbiomed.2024.03.019
41. Stockwell BR, Friedmann Angeli JP, Bayir H, et al. Ferroptosis: a regulated cell death nexus linking metabolism, redox biology, and disease. *Cell*. 2017;171(2):273–285. doi:10.1016/j.cell.2017.09.021
42. Jiang X, Stockwell BR, Conrad M. Ferroptosis: mechanisms, biology and role in disease. *Nat Rev Mol Cell Biol*. 2021;22(4):266–282. doi:10.1038/s41580-020-00324-8
43. He Q, Ma Y, Liu J, et al. Biological functions and regulatory mechanisms of hypoxia-inducible factor-1α in ischemic stroke. *Front Immunol*. 2021;12:801985. doi:10.3389/fimmu.2021.801985
44. Liu Y, Chen W, Cen Y, et al. Hepatocyte ferroptosis contributes to anti-tuberculosis drug-induced liver injury: involvement of the HIF-1α/SLC7A11/GPx4 axis. *Chem Biol Interact*. 2023;376:110439. doi:10.1016/j.cbi.2023.110439
45. Ni H, Li J, Zheng J, et al. Cardamonin attenuates cerebral ischemia/reperfusion injury by activating the HIF −1α/ VEGFA pathway. *Phytother Res*. 2022;36(4):1736–1747. doi:10.1002/ptr.7409
46. Yu P, Zhang J, Ding Y, et al. Dexmedetomidine post-conditioning alleviates myocardial ischemia-reperfusion injury in rats by ferroptosis inhibition via SLC7A11/GPX4 axis activation. *Hum Cell*. 2022;35(3):836–848. doi:10.1007/s13577-022-00682-9
47. Xu S, Li X, Li Y, et al. Neuroprotective effect of Dl-3-n-butylphthalide against ischemia-reperfusion injury is mediated by ferroptosis regulation via the SLC7A11/GSH/GPX4 pathway and the attenuation of blood-brain barrier disruption. *Front Aging Neurosci*. 2023;15:1028178. doi:10.3389/fnagi.2023.1028178